SLAC-PUB-210
September 1966

INELASTIC K^+-PROTON INTERACTIONS AT 2.65 BeV/c *

R. Newman,† W. Chinowsky and J. Schultz††
Lawrence Radiation Laboratory and Department of Physics
University of California
Berkeley, California

and

W. B. Johnson and R. R. Larsen
Stanford Linear Accelerator Center, Stanford, California

ABSTRACT

Pion production by 2.65 BeV/c K^+ mesons interacting in the BNL 20" hydrogen bubble chamber has been investigated. It is found that these inelastic events are dominated by $K^*(891)$ and $N^*(1236)$ production. Based on 537 three- and four-body events, the cross sections for production of $K^0p\pi^+$ and $K^+p\pi^+\pi^-$ are 2.7 ± 0.3 mb and 2.5 ± 0.2 mb respectively. The three body final states contain 56% K^*p and 32% N^*K^0 while the four body states contain 9% $K^*p\pi^+$, 19% $N^*K\pi^-$ and 53% K^*N^*. Resonance production is compared with predictions of several versions of the one meson exchange model. Although agreement with the data is not exact, the models tend to reproduce a number of qualitative features of the experimental results.

(To be submitted to Physical Review)

---

* Work done under the auspices of the U. S. Atomic Energy Commission.

† Present address: Columbia University, Nevis Cyclotron Lab., Irvington-on-Hudson, New York.

†† Present address: Department of Physics, University of California, Irvine, California.

I. INTRODUCTION

It has been observed that inelastic K^+- nucleon reactions have the particularly simplifying property of yielding rather small numbers of different final states, containing limited numbers of resonant particles. Since the properties of the resonances most copiously produced, $K^*(891)$ and $N^*(1236)$, are perhaps the best known of any, their production reactions are then especially suited to the study and elucidation of production dynamics. The models proposed[1] and tested[2] by comparing with data obtained at various incident K^+ momenta are variants of the simple one-pion exchange mechanism first proposed by Chew and Low[3] and Goebel.[4] There has, in general, been reasonably good qualitative agreement with the predictions of these peripheral production models, but quantitative disagreement, especially with observed absolute values of differential cross sections for the production of the resonances. Generally, for a particular reaction energy, some modification of the simple one meson exchange Born term, either by inclusion of form factors or absorption effects, can be found which will yield predictions in good agreement with the data. Of course it then becomes important to pursue the energy dependence to determine whether the modified model has any physical significance other than just arbitrary juggling of parameters to obtain better agreement with observation. To this end we present here results of a study of the reactions,

$$K^+P \rightarrow K^{*+}P \qquad (1)$$

$$K^+P \rightarrow K^{o}N^{*++} \qquad (2)$$

$$K^+P \rightarrow K^{*o}N^{*++} \qquad (3)$$

produced by K^+ mesons at an incident momentum of 2.65 BeV/c. Results for process (1) are compared with predictions of a one-meson exchange

model modified by those form factors introduced to obtain good agreement with data at other momenta. Reaction (3) will be considered with a model including absorption effects.

Again because there occur only a relatively small number of competing channels, K^+- nucleon reactions might be expected to give a good yield of any existing higher spin resonant states. Such high spin, high mass, states are to be expected if, for instance, the observed resonances are in fact to be described by "Regge" poles[5] in the complex angular momentum plane. Recurrences of the K meson might appear with mass near 1.5 BeV/c^2. The present data have been analysed to detect evidence of the existence of such states with mass up to 1.5 BeV/c^2 decaying into multibody final states.

II. EXPERIMENTAL PROCEDURE

A. Separated K^+ Beam

The experiment was conducted with the AGS accelerator and 20-in. bubble chamber at Brookhaven National Laboratory. The 20-in. chamber beam is shown schematically in Fig. 1 and is described in detail in the literature.[6] It consists of a transport and momentum-defining stage followed by two mass separation stages, the second of which provides additional momentum definition, and finally a beam shaping transport section to the chamber. The desired 2.7 BeV/c K^+ beam pressed the mass separation capability of the beam toward its limit. In order to achieve good mass separation care was taken to keep the vertical image and object sizes to a minimum. The height of the target in the AGS proton beam was .050", while the heights of slits S2, S3, and S4 in Fig. 1 were .045", .100", and .060" respectively. The πK separation achieved

is indicated in a tuning curve for the second separator, shown in Fig. 2. The run was made with the indicated setting on the high side of the K peak, where the contamination of lighter particles was negligibly small. From a comparison of the number of observed three prong K^+ decays with a count of passing beam tracks we estimate, however, a contamination .09 ± .02. As discussed below, this estimate is consistent with that obtained from fitting of the four prong events to a hypothesis with incident pion. The discrepancy we presume to result from separator instabilities causing randomly occurring periods of greatly increased pion contamination. To minimize contamination from in-flight decays of K^+ in the final section of the beam, stringent acceptance criteria were imposed on the azimuthal and dip angles of beam tracks entering the bubble chamber when selecting events for analysis. The beam momentum was determined to be (2.65 ± .03)BeV/c from measurement of passing tracks in the chamber.

B. Data Processing

A total of 50,000 pictures was taken. All film was scanned three times to locate events, providing essentially 100% scanning efficiency. Those events having a two prong topology with no observed neutral decay were not analysed in this study. Otherwise all events were measured and processed using the PANAL-PACKAGE bubble chamber analysis computer programs.[7] For the final analysis only those events occurring in a restricted fiducial volume were accepted. For each event a kinematic fit was attempted to every known combination of strongly interacting particles, consistent with the observed topology, which conserved energy, strangeness, and

baryon number, and which involved at most one unobserved particle. A hypothesis was accepted if two conditions were met: the χ^2 for the fit corresponded to a probability level greater than 1%, and the track bubble density observed was consistent with the particle velocities indicated by the fit. Ambiguities were resolved on the basis of bubble density if possible, otherwise on the basis of χ^2, except in the case of the following rather common ambiguity. Among the events with four charged prongs we often find both a four constraint fit to the final state $K^+p\pi^+\pi^-$ and a one constraint fit to $pK^+\pi^+\pi^-\pi^o$. In the latter fit the π^o is found to be nearly at rest in the laboratory frame, and the track assignments of the K^+ and p are reversed with respect to the four constraint fit. When bubble density could resolve this ambiguity, the fits positing a missing π^o were found, almost invariably, to be "fakes". Hence when bubble density could not resolve the ambiguity the fit with π^o was rejected in favor of the four constraint fit.

About 8% of the events yielded no acceptable fit. This is consistent with the number of events which might be expected to involve more than one unobserved neutral particle, together with those events arising from π contamination.

About 5% of the events were unmeasurable or failed in the computer processing after repeated tries. Channel cross sections derived from fitted events were scaled up accordingly.

Since the pion contamination in the beam is presumed small, no corrections have been made for possible pion produced events. The number of such background events which might be included in the sample because of kinematical ambiguities is a function of the particular production

channel considered. There is essentially zero effect for events with visible K^o decay. Among the four prong events, however, there is kinematical ambiguity between incident pions and K-mesons. From known pion production cross sections, we show below in more detail that the number of background events is sufficiently small to be neglected.

III. PARTIAL CROSS SECTIONS

Cross sections were determined by comparing the number of events, suitably corrected, in each channel with the number of three prong K^+ decay events occurring within the same fiducial volume and satisfying the same beam track entrance criteria. These provided a measure of the total K^+ track length. Among these events are examples of decays with Dalitz pairs as well as those via the $\pi^+\pi^+\pi^-$ mode. The branching ratio for such decays is $0.060 \pm .001$.[8] Further, a mean life $\tau_{K^+} = 1.243 \pm .004 \times 10^{-8}$ sec and hydrogen density $\rho = .0626 \pm .0003$ gm/cm^3 were used in the cross section determinations.

With a few exceptions, information on final states including a K^o or Λ^o was obtained only from those events in which the K^o or Λ^o was observed to decay within a preset volume in the chamber. To obtain cross sections, the number of such events requires two corrections. The first is a factor of 2.9 for K^o events and 1.5 for Λ^o events, to take into account the K_2^o and neutral decay modes of these particles. The second is an escape correction to allow for those K_1^o or Λ^o which decay outside the acceptance volume. This correction was made by weighting each event with a factor $w_i = (1-P_i)^{-1}$ where P_i is the probability, for that event, that the K^o or Λ^o would reach the boundary of the acceptance

volume without decaying. This is given by $P = \exp(-t/T)$, where T is the mean lifetime and t is the proper potential time available for decay. The average value of the factor w was about 1.2 for K^o decays, and 1.3 for Λ^o decays.

Cross section data for all channels accessible to this study are presented in Table I. Parentheses around a neutral particle indicate it was not observed. Errors are statistical, based on the number of events observed in each channel combined with a statistical uncertainty of 8% in the number of three prong events used to determine cross sections. Errors in the remaining quantities entering the cross section determination are negligible compared to these factors.

Table I. Cross sections for K^+p inelastic reactions at 2.65 BeV/c

Channel	Cross section (mb)
$K^o p\pi^+$	2.7 ± 0.3
$K^o p\pi^+(\pi^o)$	1.9 ± 0.2
$K^o\pi^+\pi^+(n)$	0.64 ± 0.12
$K^+p\pi^+\pi^-$	2.5 ± 0.2
$K^+p\pi^+\pi^-(\pi^o)$	0.43 ± 0.06
$K^+\pi^+\pi^+\pi^-(n)$	0.14 ± 0.03
$p\pi^+\pi^+\pi^-K^o$	0.19 ± 0.05
$p\pi^+\pi^+\pi^-K^o(\pi^o)$	0.04 ± 0.04
$K^+p\pi^+\pi^+\pi^-\pi^-$	0.01 ± 0.01
$K^+K^o\Sigma^+$	0.02 ± 0.02
$K^+K^+\Sigma^o$	$\lesssim$.01
$K^+K^+\Lambda^o$	0.03 ± 0.02
$K^+K^+\Lambda^o(\pi^o)$	0.01 ± 0.01
$K^oK^+\pi^+(\Lambda^o)$	0.03 ± 0.03

IV. ANALYSIS OF EVENTS

A. The Final State $K^o\pi^+p$

1. General features

Examples of the final state $K^o\pi^+p$ with observed K^o decay were almost without exception unambiguously identified and the effect of π^+ beam contamination is negligible. Those states produced in π^+p collisions which might be mistakenly identified are $\bar{K}^oK^+p$, $\bar{K}^oK^+p\pi^o$, $K^o\bar{K}^op\pi^+$, and $\bar{K}^oK^+n\pi^+$ which are produced with a combined cross section, at this energy, of only 0.07 mb[9] and further are easily distinguished by the quality of the fit to the kinematic constraints.

A Dalitz plot of the $K^o\pi^+p$ events is shown in Fig. 3, along with projections on the $m^2(K\pi)$ and $m^2(p\pi)$ axes. Clearly this state is dominated by the production of $K^*(891)$ and $N^*(1236)$. To estimate the relative fractions of K^* and N^* produced in this state a maximum likelihood fit was made to the Dalitz plot distribution assuming a sum of non-interfering contributions from uniform background, K^*p, and N^*K^o production:

$$I(\vec{f},m^2_{K\pi},m^2_{p\pi}) = f_1 I_B + f_2\, I_{K^*}(m_{K\pi}) + f_3\, I_{N^*}(m_{p\pi})$$

where the f_i give the relative rates into the three channels and each distribution function I is normalized to one over the Dalitz plot. I_B is a constant; Breit-Wigner forms

$$N\,\frac{\frac{m^2}{p}\,\Gamma(m)}{(m^2-m^{*2})^2 + m^{*2}\Gamma^2(m)}$$

were used for I_{K^*} and I_{N^*}. Here, letting a and b denote the products of the resonance decay, m is the effective mass of the pair ab, p is the rest frame momentum for the decay $m \to a + b$, m^* is the resonant mass, $\Gamma(m)$

is an energy dependent decay width normalized so that $\Gamma(m^*)$ is the resonance width, and N normalizes the distribution to one over the Dalitz plot. The factor m^2/p removes the phase space dependence from the Γ in the numerator. We take $\Gamma(m)$ proportional to $\frac{p^3}{m^2}$ for the K^* and proportional to $\frac{p^3}{m}(E_b+m_b)$ for the N^*, where m_b and E_b are the mass and energy respectively of the proton in the N^* rest frame. Masses and widths of the resonances were input to the fit:

$$m_{K^*} = 891,\ m_{N^*} = 1236,\ \Gamma_{K^*} = 50,\ \Gamma_{N^*} = 120\ .$$

In making the fit each event was weighted with the escape correction factor w_i defined in Section III, so that the likelihood function becomes

$$\mathcal{L}(\vec{f}) = \prod_i \left[I(\vec{f}, X_i) \right]^{w_i}$$

where X is the position on the Dalitz plot. Statistical errors, however, were estimated from a likelihood function calculated without weights. The fit indicates $(12 \pm 8)\%$ background, $(56 \pm 7)\%$ K^*p and $(32 \pm 7)\%$ N^*K^o. Curves corresponding to these values are plotted on the weighted $m^2(K\pi)$ and $m^2(p\pi)$ distributions in Fig. 3. The corresponding K^* and N^* production cross sections in this channel are $1.5 \pm .3$ mb. and $.9 \pm .2$ mb. respectively.

2. K^* Production

For the analysis of K^* production we select events with $.850 < m_{K\pi} < .930$, but not $1.16 < m_{p\pi} < 1.30$. By integrating the distributions $f_i I_i$ described in the last section we estimate this sample to be 94% K^*p, 3% N^*K, and 3% background.

The decay distribution of the K^*, in terms of its spin density matrix

is

$$w(\theta,\varphi) = \frac{3}{4\pi}\left[\rho_{00}\cos^2\theta + \rho_{11}\sin^2\theta - \rho_{1-1}\sin^2\theta\cos 2\varphi - \sqrt{2}\,\mathrm{Re}\rho_{10}\sin 2\theta\cos\varphi\right] \tag{4}$$

with $\rho_{00} = 1-2\rho_{11}$. Here θ and φ are polar angles in a coordinate system in which the y axis is taken to be normal to the production plane. If the z axis is taken to be the direction of the incident K^+ in the K^* rest frame, ρ_{00} may be interpreted as the relative contribution of pseudoscalar exchange in the framework of a one meson exchange model involving the exchange of vector and pseudoscalar particles. For π exchange $\rho_{00} = 1$ and all other elements are zero. This interpretation is not affected if the exchange process is modified by form factors. The value of ρ_{00} will be altered if absorption effects are important, but still may be expected to give an indication of the relative importance of pseudoscalar exchange.

The parameters ρ_{00} , ρ_{1-1} and $\mathrm{Re}\rho_{10}$ were evaluated from a single maximum likelihood fit to the K^* decay distribution.[10] In making this fit each event was weighted with its escape correction factor, as in the fit to the Dalitz plot distribution. To avoid biases arising from the omission of the part of the K^* band which overlaps the N^* band, we exploit the fact that distribution (4) is invariant under the transformation $\theta \to \pi - \theta$, $\varphi \to \varphi + \pi$. The overlap is so located that if an event lies in the overlap region, then its conjugate event lies outside it.[11] In making the fit each event was given a weight factor of two if its conjugate lay in the overlap region, thus effectively replacing the excluded events. There result the following density matrix elements:

$$\rho_{00} = 0.20 \pm 0.08$$
$$\rho_{1,-1} = 0.19 \pm 0.09$$
$$\mathrm{Re}\rho_{10} = -0.16 \pm 0.03$$

Evidently the data are not consistent with a pion exchange mechanism. Figure 4 shows the measured and fitted decay angular distributions.

As has been observed from results at other energies, the K^* production angular distribution, seen in Fig. 5, is strongly peaked at forward angles, a feature characteristic of production in peripheral collisions. We consider then the application of a one meson exchange model, modified with inclusion of form factors, following Jackson and Pilkuhn.[12] With a restriction to low mass particles, the exchange of π, η, ρ, ω and ϕ mesons is allowed. We argue that only π and ω exchange need be taken into account. Evidence against importance of ρ exchange has been provided by the results of a study[13] of the reaction $K^+n \to K^{*o}p$ in which isoscalar meson exchange is forbidden. Isospin invariance applied at the vertices of the exchange diagram permits us to conclude that ρ exchange does not contribute significantly to the K^+p reaction. The absence of ρ exchange provides some support for the conservation of A parity,[14] which forbids a ρKK^* coupling. Conservation of A parity would also forbid a φKK^* coupling. This, along with the high mass of the φ, provides arguments against the importance of φ exchange in our reaction. As for the η, SU_3 symmetry using a D/F ratio of 2.0 indicates $g^2_{pp\eta}/g^2_{pp\pi^o} = \frac{1}{27}$, while at the meson vertex we have $g^2_{KK^*\eta}/g^2_{KK^*\pi^o} = \frac{1}{3}$. This, along with the high mass of the η compared to the π^o, indicates that the contribution of η exchange to our reaction will be small compared to π exchange. Hence we restrict our model to the exchange of π and ω mesons. Treating the K^* as a stable particle, we may write its production cross section with the one meson exchange

model (OME) as

$\frac{d\sigma}{d\Omega} = \frac{d\sigma_p}{d\Omega} + \frac{d\sigma_v}{d\Omega}$ where, with a factor for the $K^* \to K^o\pi^+$ branching ratio,

$$\frac{d\sigma_p}{d\Omega} = \frac{2q'}{3sq} \frac{g^2}{4\pi} \frac{G^2}{4\pi} \Delta^2 a_c^2 \left| \frac{F_p(\Delta^2)}{m_\pi^2+\Delta^2} \right|^2$$

is the contribution from π exchange, and

$$\frac{d\sigma_v}{d\Omega} = \frac{q'}{3sq} \frac{f^2}{4\pi} \left| \frac{F_v(\Delta^2)}{M_v^2+\Delta^2} \right|^2 \left[\frac{(G_v+G_T)^2}{4\pi} \Delta^2 a_c^2 + \frac{2sq^2q'^2\sin^2\theta}{M_{K^*}^2} \left(\frac{G_v^2}{4\pi} + \frac{G_T^2}{4\pi} \frac{\Delta^2}{4M_p^2} \right) \right]$$

is the contribution from vector meson exchange. Here a_c is the momentum of the incident K^+ in the rest frame of the K^*,

$$a_c^2 = \frac{1}{4M_{K^*}^2} \left[\Delta^2 + (M_K - M_{K^*})^2 \right] \left[\Delta^2 + (M_K + M_{K^*})^2 \right]$$

s is the square of the C.M. energy, q is the C.M. momentum of the K^+, q' is the C.M. momentum of the K^*, and Δ^2 is the momentum transfer to the K^*. In the π exchange contribution $\frac{g^2}{4\pi}$ is the $K^+\pi^oK^{*+}$ coupling constant, estimated from the K^* decay width to be about .75, $\frac{G^2}{4\pi} \approx 15$ is the $NN\pi^o$ coupling constant, and $F_p(\Delta^2)$ is a form factor. In the vector exchange contribution $\frac{f^2}{4\pi}$ is the vector meson coupling constant at the KK^* vertex, G_V and G_T are coupling constants at the nucleon vertex, and $F_v(\Delta^2)$ is a form factor. Of the vector coupling constants little is known, except that one can argue[9] for ω exchange that $G_T \approx 0$. The unknowns then in these expressions are the product $f^2G_V^2$ and the two

form factors $F_p(\Delta^2)$ and $F_v(\Delta^2)$.

To apply the model to the present results, we adopt parameters induced from experimental results at other energies. Thus we use the form factors

$$F_v(\Delta^2) = \exp[-\Delta^2/0.7] \quad \text{and}$$

$$F_p(\Delta^2) = (\gamma^2 - m_\pi^2)/(\gamma^2+\Delta^2) \ ,$$

with $\gamma^2 = 0.165(\text{BeV/c})^2$ and Δ^2 is in $(\text{BeV/c})^2$. The first was used in analysing K^* production data from 3.0 BeV/c interactions.[15] The pseudoscalar form factor was obtained in the analysis of results[16] at 1.96 BeV/c, and from the K^*N^* production data at 1.96 BeV/c[17] and 3.0 BeV/c.[18]

In Fig. 5 we show the K^* production angular distribution together with the distribution predicted by the one-meson exchange model in the form given. To obtain quantitative agreement with the measured differential cross section, a coupling constant $(f^2 G_v^{\,2})/(4\pi)^2 = 28.6$ is required. This value is in disagreement with that obtained from a fit to the 3.0 BeV/c data, $(f^2 G_v^{\,2})/4\pi = 13.4$, as can be seen directly from the corresponding curve a of Fig. 5.

Total $K^+p \to K^*p$ cross sections from a number of experiments are plotted as a function of incident momentum in Fig. 6. Curves a and b have the same meaning as before. Curves c and d are respectively the π and ω exchange contributions to curve a . Here we see very dramatically the failure of the simple OME model to reproduce the energy dependence of the K^* production cross section. The predicted cross section rises steadily, while experimentally it rises steeply at threshold and then falls off rapidly. This experimental behavior corresponds closely to that of the total cross section for the channel $K^0\pi^+p$, which is shown in Fig. 7. The falling off of this cross section becomes understandable

when we note that the total K^+p cross section above K^* threshold is nearly constant, so that the opening up of new multibody channels is necessarily at the expense of the $K^0\pi^+p$ cross section, and hence of the K^*p cross section. Thus it becomes quite clear that a model for K^*p production must take into account the effect of competing channels.

From Fig. 6 we see that the rise of the OME cross section with energy results from the vector exchange contribution. This increase with energy is a well known difficulty associated with vector exchange models. As we see here, this behavior is not controlled by the addition of a form factor. Unfortunately, it is also not tamed satisfactorily by the absorption model as formulated by Jackson and others.[26,27]

Next we compare in Fig. 8 the observed values of the density matrix parameter ρ_{00} at several production momenta with the predictions of the model. The values of ρ_{00} are averaged over momentum transfer, and as indicated earlier give a measure of the relative importance of pseudoscalar exchange. Curves a and b have the same meaning as before. Here the simple OME model gives a somewhat more accurate prediction.

Finally we note that the OME model used above implies a zero value of the density matrix parameter $\mathrm{Re}\rho_{10}$, although inclusion of absorption effects predicts in general a nonzero value. In fact we find that parameter to be $-.16 \pm .03$, indicating another failure of the simple model we have applied.

In conclusion we state that the OME model modified only by form factors gives rather poor agreement with the data on the reaction $K^+p \to K^*p$. Production angular distributions are reproduced only by fitting with drastic form factors of rather arbitrary form, while the

energy dependence of the reaction cross section is reproduced very badly. It is not likely that the inclusion of η or φ exchange contributions could alter this conslusion.

3. N^* Production

For analysis of the N^* production reaction we select events within the previously defined $M(p\pi)$ limits and exclude events with $M(K^o\pi^+)$ within the limits defining K^*. Figure 9 shows the N^* production and decay angular distributions. Again a strong peaking at low momentum transfer is observed. Comparision with models for the production distribution has not been made, because of the limited statistical validity of the data.

The N^* decay angular distribution in terms of the elements of its spin density matrix is

$$w(\theta,\varphi) = \frac{3}{4\pi}\left[\rho_{33}\sin^2\theta + \rho_{11}\left(\frac{1}{3} + \cos^2\theta\right) - 2/\sqrt{3}\ \mathrm{Re}\rho_{3-1}\sin^2\theta\cos 2\varphi - 2/\sqrt{3}\ \mathrm{Re}\rho_{31}\sin 2\theta\cos\varphi\right] \qquad (5)$$

where the coordinate system is defined with the y axis normal to the production plane. Here $\rho_{11} = 1/2 - \rho_{33}$. Angles θ, φ are defined in this system as shown in Fig. 9. The data plotted in Fig. 9 have been corrected for K^o escape and for omission of events in the K^*-N^* overlap region as described in the preceding section. The N^* density matrix elements obtained from a single maximum likelihood fit to the decay distribution in space are

$$\rho_{33} = 0.50 \pm 0.10$$
$$\mathrm{Re}\rho_{3-1} = 0.19 \pm 0.07$$
$$\mathrm{Re}\rho_{31} = 0.09 \pm 0.07$$

The distributions in $\cos\theta$ and φ given by (2) using the density matrix elements determined from the maximum likelihood fit are shown in comparison with the observed distributions in Fig. 9.

It is interesting to note that the number of "conjugate" events used to replace the N^* events in the overlap region of the K^* and N^* bands, plus the corresponding number of events for the K^* sample, is seven--exactly the number of events which actually lie in the overlap region for our sample. The number of events predicted by integrating the distribution of our fit over the overlap region is 8. Thus it appears that there is neither constructive nor destructive interference between K^* and N^* amplitudes in the overlap region.

B. The Final State $K^+p\pi^+\pi^-$

1. General features

We consider first the effect of pion contamination in the beam on the sample of events identified as examples of the reaction $K^+p \to K^+p\pi^+\pi^-$. These are indistinguishable from background events produced in the reaction $\pi^+p \to \pi^+p\ \pi^+\pi^-$ if one of the final state positive pions has a momentum comparable to the beam momentum. In fact some 25% of the 471 events were consistent with the kinematics of either incident π^+ or K^+. We assume that the fitting procedure for pion produced events in the state $\pi^+\pi^+p\pi^-$ yields a similar fraction of ambiguous fits. With a total of 39 ± 7 four prong events fitting only pion-production kinematics, taking into account that it is sufficient that either π^+ be of high momentum to simulate a K^+ event, we find a fraction 0.06 ± .01 of the sample to be pion contamination. This yields, with cross sections 3.5 mb[28] and 2.5 mb respectively

for the π^+ and K^+ reactions, a beam background $.095 \pm .015$, consistent with the estimate based on beam decay counts. In the analysis of the data, this background is neglected.

In Fig. 10 we present a triangle plot of the observed $K^+\pi^-$ and $p\pi^+$ masses. Abundant production of K^* and N^* is clearly indicated. To determine the relative rates of the reactions yielding K^*, N^*, K^* with N^* and non-resonating particles, a maximum likelihood fit was made to the intensity distribution within the triangle plot boundaries. Assuming the total amplitude for the reaction to be a sum of non-interfering amplitudes for the four processes, this distribution is

$$I\left(\vec{f}, M_{K\pi^-}, M_{p\pi^+}\right) = \left\{ f_1 I_{K^*N^*} + f_2 I_{K^*} + f_3 I_{N^*} + f_4 I_B \right\} pq_1q_2/W \qquad (6)$$

Here I_{K^*} and I_{N^*} have the functional dependence on $M_{K\pi^-}$ and $M_{p\pi^+}$, respectively, given in Section IV.A. The distribution function $I_{K^*N^*} = \text{const} \times I_{K^*}I_{N^*}$, while I_B is constant. Multiplying each term in brackets is the phase space factor associated with a point within the triangle, with p the momentum of the $p\pi^+$ pair in the overall c.m. system, q_1 the momentum of the π^+ in the $p\pi^+$ rest system, q_2 the momentum of the π^- in the $K^+\pi^-$ rest system and W the total energy in the center of mass system. Each of the four distribution functions is independently normalized to give, when multiplied with the phase space factor, unit integral over the triangle. The factors f_i give the relative rates into the four final states, with of course $\Sigma f_i = 1$.

This procedure yielded the relative production rates via the four channels:

$K^{*o}N^{*++}$	0.53 ± 0.04
$K^{*o}p\pi^+$	0.09 ± 0.04
$N^{*++}K^+\pi^-$	0.19 ± 0.04
$K^+p\pi^+\pi^-$	0.19 ± 0.04

Mass distributions of $K^+\pi^-$ and $p\pi^+$ pairs obtained with these rates and the functional form above are plotted on the projections of the scatter plot in Fig. 10.

2. Production of K^*N^*

To study the details of the reaction $K^+p \rightarrow K^*N^*$, we select those events for which $.85 < m_{K\pi^-} < .93$ and $1.12 < m_{p\pi^+} < 1.34$. By integrating separately the four terms in distribution (6) over this region of the triangle plot we estimate the sample to contain 82% K^*N^* events, 7% $K^*p\pi^+$, 7% $N^*K^+\pi^-$, and 4% non-resonant background, assuming no interference between these contributions. Using our estimate that the pion-produced background included in the total sample of events is less than 7%, and assuming that such events are distributed over the "triangle" plot roughly according to phase space, we estimate that the number of pion produced events included in the sample defined above is less than $\frac{1}{2}$% of that sample.

General expressions for the decay distributions of the K^* and N^* in terms of their spin density matrix elements were given previously. Those parameters for our sample of K^*N^* production, were evaluated using a three parameter maximum likelihood fit to the decay distributions of the K^* and N^* with the coordinate systems defined in Figs. 11 and 12. Results are presented in Table II for the total sample, and for subsamples corresponding to different regions of production angle. In Figs. 11 and 12 we present the decay distributions of the K^* and N^* respectively, along with curves determined by the density matrix elements obtained from the fit to the complete sample. While these density matrix parameters are not consistent with predictions of

the simple one pion exchange model, which requires $\rho_{00} = 1$ and all other matrix elements in Table II zero, the disagreement is not overwhelming.

Further evidence for the dominance of single particle exchange is again provided by the production angular distribution, shown in Fig. 13. This distribution also is sharply peaked at small momentum transfers, with the K^* preferentially in the forward direction. Since the decay distributions are almost consistent with the unmodified one pion exchange model predictions, but the production process is peripheral, we now compare the data with a single π-meson exchange model including absorption.

Using the formulation of the model given by Jackson and others[26] we obtain, for the K^*N^* production at small angles, a helicity amplitude

$$< \lambda_{K^*} \lambda_{N^*} | M | \lambda_p > = A_n \int_{j_o}^{\infty} J_n(\alpha x) k(x - \tfrac{1}{2}) x \, dx + \sum_{j=j_o}^{j_{max}} \bar{A}_{nj} d_{\lambda\mu}(\theta) k(j) \qquad (7)$$

where the notation is that of the reference cited. This expression differs from that of reference 26 in that the sum includes a term with $j = 3/2$ as well as the term with $j = j_0 = 1/2$ and we use $k(j)$ rather that $k(j - \frac{1}{2})$. Results are presented for both forms. The absorption effects are contained in the functions

$$k(j) = e^{i\delta_j^+} e^{i\delta_j^-}$$

Table II K^* and N^* density matrix parameters in the reaction $K^+p \to K^{*o}N^{*++}$ for various ranges of production angle θ.

K^*	$\cos\theta$	Δ^2	ρ_{00}	$\rho_{1,-1}$	$Re\rho_{10}$
	.95 - 1.0	.13 - .19	0.90 ± 0.16	-0.22 ± 0.06	-0.18 ± 0.07
	.90 - .95	.19 - .26	1.00 ± 0.12	0.14 ± 0.08	-0.18 ± 0.04
	.80 - .90	.26 - .39	0.36 ± 0.12	-0.04 ± 0.10	-0.17 ± 0.06
	-1.0 - .80	.39 -2.68	0.58 ± 0.10	-0.08 ± 0.07	-0.10 ± 0.06
	-1.0 - 1.0	.13 -2.68	0.65 ± 0.06	-0.07 ± 0.04	-0.16 ± 0.04

N^*	$\cos\theta$	Δ^2	ρ_{33}	$Re\rho_{3,-1}$	$Re\rho_{31}$
	.95 - 1.0	.13 - .19	0.24 ± .09	-0.01 ± 0.08	-0.10 ± 0.10
	.90 - .95	.19 - .26	0.00 ± 0.11	0.07 ± 0.09	0.09 ± 0.09
	.80 - .90	.26 - .39	0.26 ± 0.09	-0.06 ± 0.09	0.00 ± 0.10
	-1.0 - .80	.39 -2.68	0.18 ± 0.07	0.05 ± 0.07	-0.10 ± 0.08
	-1.0 - 1.0	.13 -2.68	0.18 ± 0.05	0.01 ± 0.04	-0.04 ± 0.05

where δ_j^+ and δ_j^- are the complex elastic scattering phase shifts in the initial and final channels. Again, Jackson's form is used for these:

$$e^{i\delta_j^\pm} = \left[1 - C_\pm e^{-\gamma_\pm j^2}\right]^{1/2}$$

with $C_+ = \sigma_T^+/4\pi A_+$ and $\gamma_+ = 1/2\, q^2 A_+$, where σ_T^+ is the total K^+p scattering cross section, q the incident c.m. momentum and A the logarithmic derivative of the differential cross section, assumed of the form

$$\sigma(t) = \sigma_o e^{At}$$

Further, it is assumed that $C_+ = C_-$. Calculations were made with $\gamma_+ = \gamma_-$ and also $\gamma_- = \gamma_+/3$.

To evaluate C_+ and γ_+, a total cross section of 17_{mb}[29] was used; A^+ was obtained by interpolating from results at other energies,[30, 31] yielding $A^+ \sim 3.5$. We then obtain $C_+ = 1.0$ and $\gamma_+ = 0.15$.

In Fig. 14 we show the absorption model predictions for the K^*N^* production angular distribution near the forward direction, compared with our experimental data. Curve a is the prediction of the unmodified single pion exchange model, while curve b is the prediction of the absorption model with the parameters defined above. Curve b reproduces the shape of the experimental distribution, but is about a factor of 2 too high in magnitude. For comparison we present curve c, which is the result of a calculation in which the range of the absorption in the final state has been increased by putting $\gamma_- = .05$, and curve d, which results from replacing k(j) with $k(j - \frac{1}{2})$ in the sum of Eq. 7, following Jackson. In Fig. 15 we compare absorption model predictions with our data on the K^* and N^* density matrix parameters as a function of production angle. In each plot the solid curve corresponds to a calculation with $C_+ = C_- = 1.0$, $\gamma_+ = \gamma_- = .15$. Putting

$\gamma_- = .05$ leads to curves almost identical to these. The dashed curves are the result of replacing $k(j)$ with $k(j - \frac{1}{2})$ in Eq. 7.

The agreement of the data on K^*N^* production with the predictions of the absorption model is not very good. However the model does roughly reproduce the production differential cross section, and succeeds generally in reproducing the sign and order of magnitude of the deviations of the density matrix parameters from the values predicted by the unmodified theory. A virtue of the model is that it involves no arbitrary parameters to be determined by "fitting."

One of the problems with the absorption model is the crude way in which the absorption factors must be represented as a function of j. In fact, as pointed out by Jackson,[26] the absorption might more reasonably be taken to be a decreasing function of the orbital angular momentum ℓ . For the production K^*N^* (or ρN^*) the values of ℓ can differ from the corresponding values of j by as much as $5/2$, and the relations between ℓ and j are of course quite complicated. This may be a serious problem, since the results of absorption model calculations seem to be quite sensitive to the way that absorption is introduced in the low partial waves. This may be seen in comparing our results using $k(j)$ and $k(j - \frac{1}{2})$ in the sum of Eq. 7. This sensitivity has also been found, especially for production angular distributions, in a detailed study of some cases by Högaasen et al.[32]

V. SEARCH FOR OTHER RESONANT STATES

We have examined all 2 and 3 body effective mass distributions in the channels

$$K^+p \rightarrow K^+p\,\pi^+\pi^- \qquad \text{(400 events)} \qquad (8)$$

$$K^+p\,\pi^+\pi^-\pi^o \qquad \text{(77 events)} \qquad (9)$$

and find no evidence for the production of resonant states other than $K^*(891)$, $N^*(1236)$, and ω . The cross section for ω production in channel (9) above is 0.07 ± 0.03 mb.

We have looked particularly for possible enhancements in the $K\,\pi\,\pi$ mass distributions in these channels. In Fig. 16 we show the $K^+\pi^+\pi^-$ mass distribution in channel (8). The dashed curve is the phase space distribution, while the solid curve is the distribution which would result from the production of K^* and N^* in the proportions indicated in Section IV, assuming simple Breit-Wigner forms for their production matrix elements, and assuming that these resonances decay isotropically. The experimental distribution deviates from both curves near 1.2 BeV/c . A much sharper $K\,\pi\,\pi$ enhancement has been reported in π^-p reactions at a mass of 1.175 BeV/c .[33] Further, no such enhancement is found in the corresponding mass distributions of the five body events of channel (9). Hence it is concluded that the $K^+\pi^+\pi^-$ enhancement in the four body states is a kinematical effect, perhaps reflecting non-isotropic decays of the K^* and N^* resonant states.

The observation of a small peak in K^+p and K^+n total cross sections at a C.M. energy of about 1.19 BeV has raised the possibility of a $Y = 2$, $B = 1$, $I = 1$ resonant state with that mass and a width $\Gamma \approx 180$ MeV.[34] We have examined the K^+p and $K^+p\pi^o$ distributions in the above channels for such an enhancement. We find no statistically valid evidence for production of such a state.

ACKNOWLEDGEMENTS

We wish to acknowledge the assistance of the members of the BNL Bubble Chamber Group and the AGS staff for their aid in making this experiment possible.

REFERENCES

1. N. J. Sopkovich, Nuovo Cimento 26 186 (1962)
L. Durand and Y. Y. Chiu, Phys. Rev. 139, B646 (1965)
K. Gottfried and J. D. Jackson, Nuovo Cimento 34, 735 (1964)
E. Ferrari and F. Selleri, Nuovo Cimento Suppl. 24, 453 (1962)
L. Stodolsky and J. J. Sakurai, Phys. Rev. Letters 11, 90 (1963)
See also refs. 2 and 26 below for reviews containing extensive references.

2. The review article by J. D. Jackson, Rev. Mod. Physics 37, 484 (1965) gives many references to experimental results. See also refs. 10, 12-19 below.

3. G. F. Chew and F. E. Low, Phys. Rev. 113, 1640 (1959).

4. C. J. Goebel, Phys. Rev. Letters 1, 337 (1958).

5. T. Regge, Nuovo Cimento 14, 951 (1959).
G. F. Chew and S. C. Frautschi, Phys. Rev. Letters 7, 394 (1961) and ibid 8, 41 (1962).

6. C. Baltay, J. Sandweiss, J. Sanford, H. Brown, M. Webster, and S. Yamamoto, Nucl. Instr. Methods 20, 37 (1963); J. Leitner, G. Moneti, and N. P. Samios, ibid. 20, 42 (1963).

7. W. E. Humphrey and A. H. Rosenfeld, Ann. Rev. Nucl. Sci. 13, 103 (1965); A. H. Rosenfeld, UCRL-9099 (1961), Lawrence Radiation Laboratory, Berkeley.

8. G. Trilling, UCRL-16473 (November, 1965).

9. D. Berley and N. Gelfand, Phys. Rev. 139, B1097 (1965).

10. It should be noted that the sign of the density matrix parameter $\mathrm{Re}\rho_{10}$ for the K^* and $\mathrm{Re}\rho_{31}$ for the N^* depends on the choice of the normal to the production plane. We take always $\hat{n} = (q \times q')$ where q is the momentum of the incident K^+, and q' is the momentum of the K^* in the final states K^*p and K^*N^*, or of the K^o in the final state K^oN^*.

11. P. Eberhard and M. Pripstein, Phys. Rev. Letters 10, 351 (1963).

12. J. D. Jackson and H. Pilkuhn, Nuovo Cimento 33, 906 (1964); 34, 1841E (1964).

13. S. Goldhaber, J. L. Brown, I. Butterworth, G. Goldhaber, A. A. Hirata, J. A. Kadyk, and G. H. Trilling, Phys. Rev. Letters 15, 737 (1965).

14. J. B. Bronzan and F. E. Low, Phys. Rev. Letters 12, 522 (1964).

15. M. Ferro-Luzzi, R. George, Y. Godschmidt-Clermont, V. P. Henri, B. Jongejans, D. W. G. Leith, G. R. Lynch, F. Muller and J.-M. Perreau, Nuovo Cimento 36, 1101 (1965).

16. S. Goldhaber, W. Chinowsky, G. Goldhaber, and T. O'Halloran, Phys. Rev. 142, 913 (1966).

17. G. Goldhaber, W. Chinowsky, S. Goldhaber, W. Lee, and T. O'Halloran, Phys. Letters 6, 62 (1963).

18. M. Ferro-Luzzi, R. George, Y. Goldschmidt-Clermont, V. P. Henri, B. Jongejans, D. W. G. Leith, G. R. Lynch, F. Muller, and J.-M. Perreau, Nuovo Cimento 39, 417 (1965).

19. M. G. Bowler, R. W. Bland, J. L. Brown, G. Goldhaber, J. A. Kadyk, V. Seeger, and G. H. Trilling; Paper presented at the Oxford International Conference on Elementary Particles (1965), and UCRL-16370 (December, 1965), Lawrence radiation Laboratory, Berkeley.

20. E. Boldt, J. Duboc, N. H. Duong, P. Eberhard, R. George, V. P. Henri, F. Levy, J. Poyen, M. Pripstein, J. Cussar, and A. Tran, Phys. Rev. 133, B220 (1964).

21. G. B. Chadwick, D. J. Crennell, W. T. Davies, M. Derrick, J. H. Mulvey, P. B. Jones, D. Radojicic, C. A. Wilkinson, A. Tettini, M. Cresti, S. Limentani, L. Poruzzo, and R. Santangelo, Phys. Letters 6, 309 (1963). See also Ref. 15 and references given therein.

22. B. Kehoe, Phys. Rev. Letters 11, (1963).

23. R. W. Bland, M. G. Bowler, J. L. Brown, G. Goldhaber, S. Goldhaber, J. A. Kadyk, V. H. Seeger and G. H. Trilling, private communication.

24. The value of ρ_{oo} at P_{Lab} = 1.45 BeV/c in Fig. 8 is based on an estimate of the pseudoscalar exchange contribution given in Ref. 18.

25. B. C. Shen, I. Butterworth, C. Fu, G. Goldhaber, S. Goldhaber, S. L. Hagopian and G. H. Trilling, private communication.

26. J. D. Jackson, J. T. Donohue, K. Gottfried, R. Keyser and B. E. Y. Svensson, Phys. Rev. 139, B428 (1965).
Extensive references to other work on "absorption models" will be found in this paper.

27. H. Hogaasen and J. Hogaasen, Nuovo Cimento 39, 941 (1965).

28. C. Alff-Steinberger, D. Berley, D. Colley, N. Gelfand, D. Miller, U. Nauenberg, J. Schultz, T. H. Tan, H. Brugger, P. Kramer, and R. Plano, Phys. Rev. 145, 1072 (1966).

29. V. Cook, D. Keefe, L. T. Kerth, P. G. Murphys, W. A. Wenzel, and T. F. Zipf, Phys. Rev. Letters 7, 182 (1961).

30. W. Chinowsky, G. Goldhaber, S. Goldhaber, T. O'Halloran, and B. Schwarzchild, Phys. Rev. 139, B1411 (1965).

31. J. Debaisieux, F. Grard, J. Heughebaert, L. Pape, R. Windmolders, R. George, Y. Goldschmidt-Clermont, V. P. Henri, D. W. G. Leith, G. R. Lynch, F. Muller, J.-M. Perreau, G. Otter, and P. Sallstrom, Nuovo Cimento 43, A142 (1966).

32. H. Hogaasen, J. Hogaasen, R. Keyser, and B. E. Y. Svensson, Nuovo Cimento 42, A323 (1966).

33. T. P. Wangler, A. R. Erwin, W. D. Walker, Phys. Letters 9, 71 (1964); D. H. Miller, A. Z. Kovacs, R. L. McIlwain, T. R. Palfrey, and G. W. Tautfest, Phys. Letters 15, 74 (1965).

34. R. L. Cool, G. Giacomelli, T. F. Kycia, B. A. Leontic, K. K. Li, A. Lundby, and J. Teiger, Phys. Rev. Letters 17, 102 (1966).

FIGURE CAPTIONS

Fig. 1 Schematic diagram of the beam to the Brookhaven 20" bubble chamber.

Fig. 2 Beam tuning curve, indicating π-K mass separation achieved. Counting rate at the second mass separation slit (S4) is plotted vs. magnetic field in the second mass spectrometer.

Fig. 3 Dalitz plot for the final state $K^{o}p\pi^{+}$. Events in the mass histogram are weighted as described in the text. Curves plotted on the histograms correspond to the production of $K^{*}(891)$, $N^{*}(1236)$, and non-resonant background in proportions determined from a likelihood fit to the Dalitz plot distribution.

Fig. 4 Decay angular distributions for the K^{*} in the channel $K^{*+}p$. Particle symbols in the coordinate system diagram represent the direction of motion of the particles in the K^{*} rest frame. Events are weighted as described in the text. Curves are determined by K^{*} density matrix parameters obtained from a three parameter likelihood fit to the (θ,φ) distribution.

Fig. 5 K^{*} production angular distribution for the reaction $K^{+}p\rightarrow K^{*+}p$. The curves are predictions of a one meson exchange model modified by form factors, with π and ω exchange. Values of the vector coupling constant $f^{2}G_{V}^{2}$ are chosen to reproduce the $K^{*+}p$ total cross section at 3.0 BeV/c (curve a) and 2.65 BeV/c (curve b).

Fig. 6 Energy dependence of the cross section for the reaction $K^{+}p\rightarrow K^{*+}p$, $K^{*+}\rightarrow K^{o}\pi^{+}$. Curves a and b have the same meaning as in Fig. 5, while curves c and d represent the π and ω exchange contributions to curve a.

Fig. 7 Energy dependence of the cross section for the reaction $K^+p \to K^o\pi^+p$.

Fig. 8 Energy dependence of the K^* density matrix element ρ_{00} in the reaction $K^+p \to K^*p$. Curves a and b have the same meaning as in Fig. 5.

Fig. 9 Production and decay distributions for the N^* in the channel $N^{*++}K^o$. Particle symbols in the coordinate system diagram represent the direction of motion of the particles in the N^* rest frame. Events in the decay distributions are weighted as described in the text. Curves are determined by N^* density matrix parameters obtained from a fit to the (θ,φ) distribution.

Fig. 10 Mass scatterplot for the final state $K^+p\pi^+\pi^-$. Curves plotted on the mass histograms correspond to the production of K^*N^{*++}, K^{*o}, N^{*++}, and non-resonant background in proportions determined from a likelihood fit to the scatterplot distribution.

Fig. 11 Decay angular distributions for the K^* in the channel $K^{*o}N^{*++}$. Particle symbols in the coordinate system diagram represent the direction of motion of the particles in the K^* rest frame. Curves are determined by K^* density matrix parameters obtained from a three parameter likelihood fit to the (θ,φ) distribution.

Fig. 12 Decay angular distributions for the N^* in the channel $K^{*o}N^{*++}$. Particle symbols in the coordinate system diagram represent the direction of motion of the particles in the N^* rest frame. Curves are determined by N^* density matrix parameters obtained from a three parameter likelihood fit to the (θ,φ) distribution.

Fig. 13 Production angular distribution of the K^* in the reaction $K^+p \to K^{*o}N^{*++}$, $K^* \to K^+\pi^-$. The curve represents a pion exchange model modified only by a form factor.

Fig. 14 Production angular distribution of the K^* in the reaction $K^+p \to K^{*o}N^{*++}$, $K^* \to K^+\pi^-$. Curve a is the prediction of the unmodified pion exchange model; curves b, c, and d follow from π exchange modified by absorption as discussed in the text.

Fig. 15 Density matrix parameters, as a function of production angle, for the K^* and N^* in the reaction $K^+p \to K^{*o}N^{*++}$. Curves are the predictions of an absorption model, as described in the text.

Fig. 16 $M(K^+\pi^+\pi^-)$ distribution in the channel $K^+p\,\pi^+\pi^-$. The dashed curve is the phase space distribution, while the solid curve represents the effect of production of K^{*o} and N^{*++}, as described in the text.

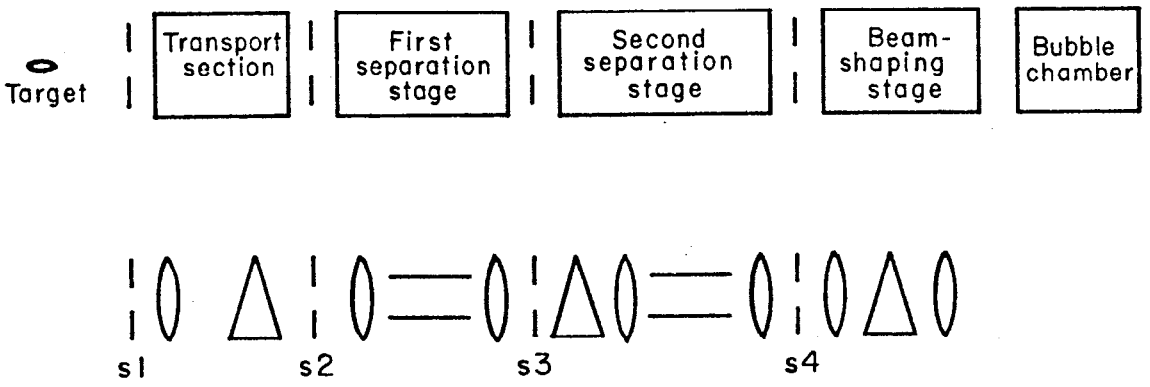
Target
Transport section
First separation stage
Second separation stage
Beam-shaping stage
Bubble chamber
s1
s2
s3
s4
MUB-11440

Figure 1

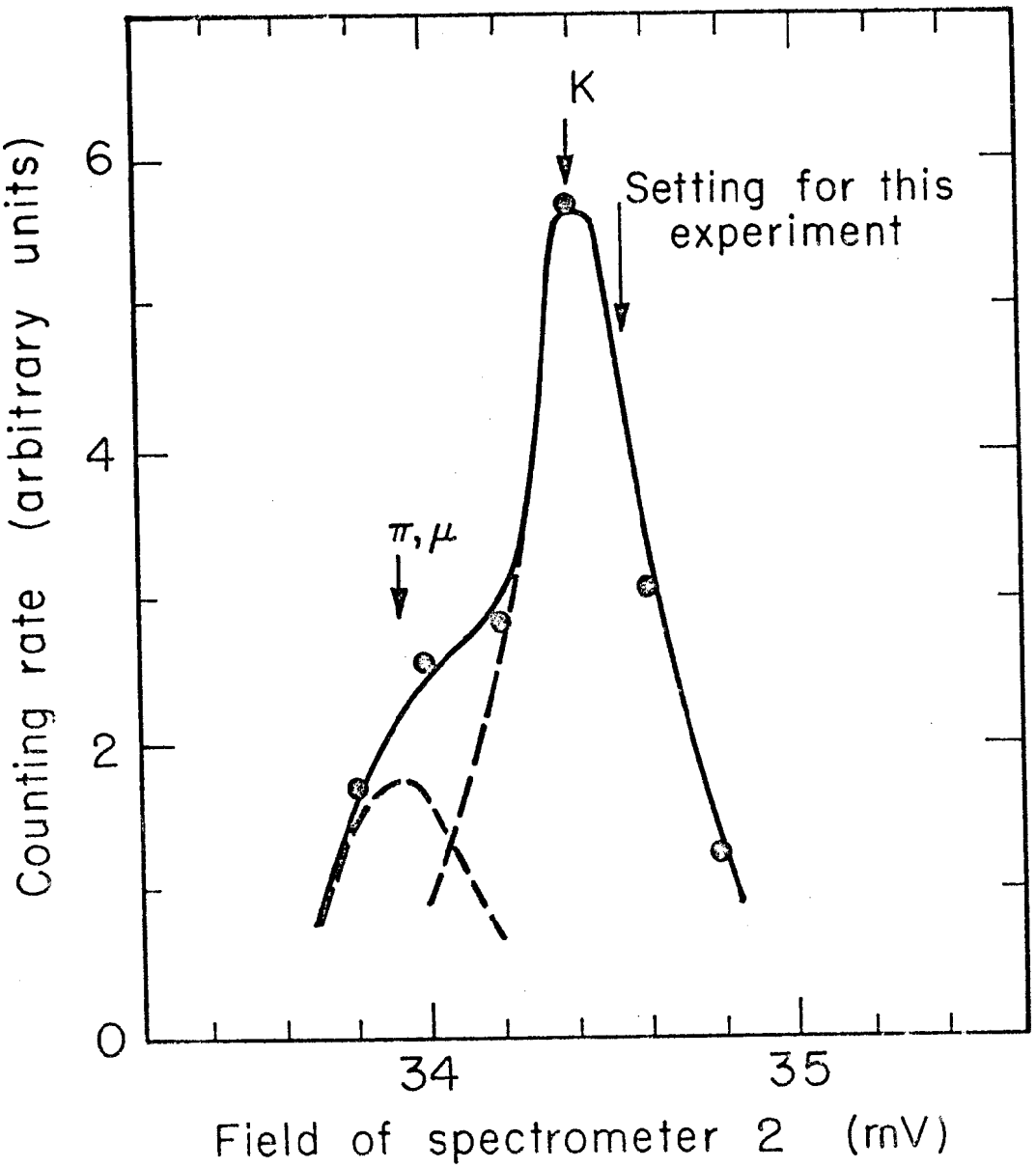

MUB-11443

Figure 2

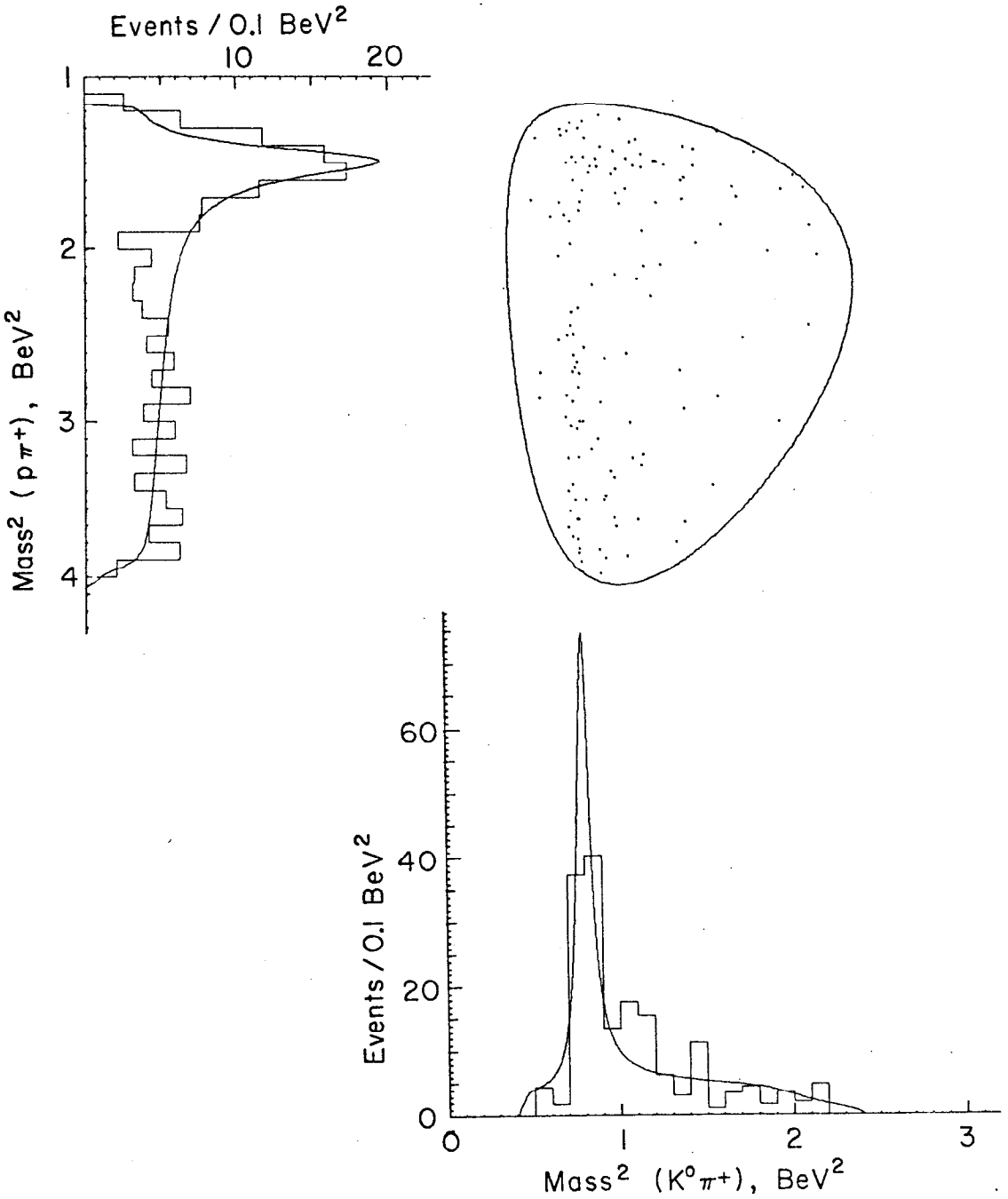
Events / 0.1 BeV²
10
20
1
2
3
4
Mass² (pπ⁺), BeV²
60
40
20
0
0
1
2
3
Events / 0.1 BeV²
Mass² (K°π⁺), BeV²
MUB-11445

Figure 3

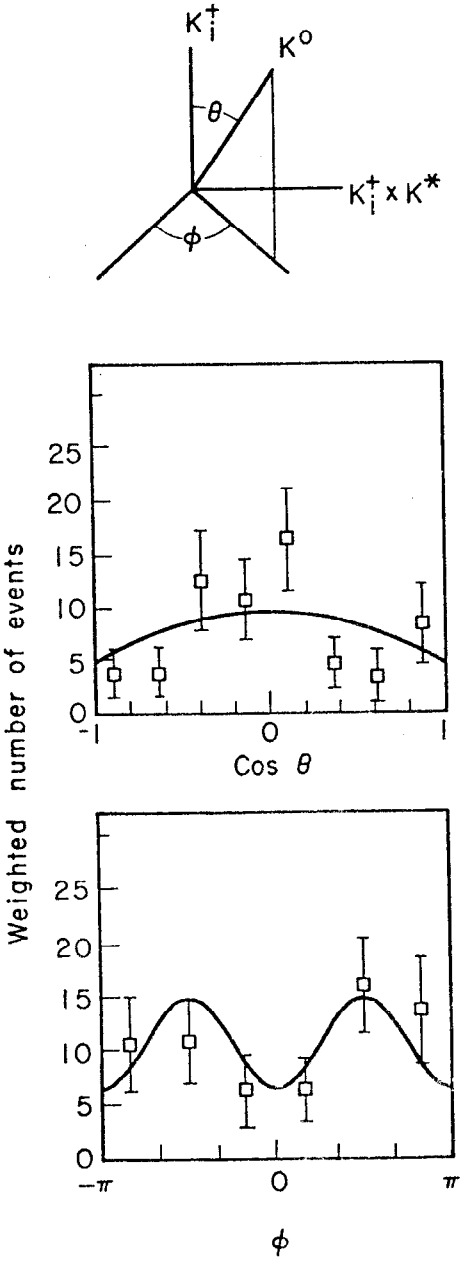

MUB-11405

Figure 4

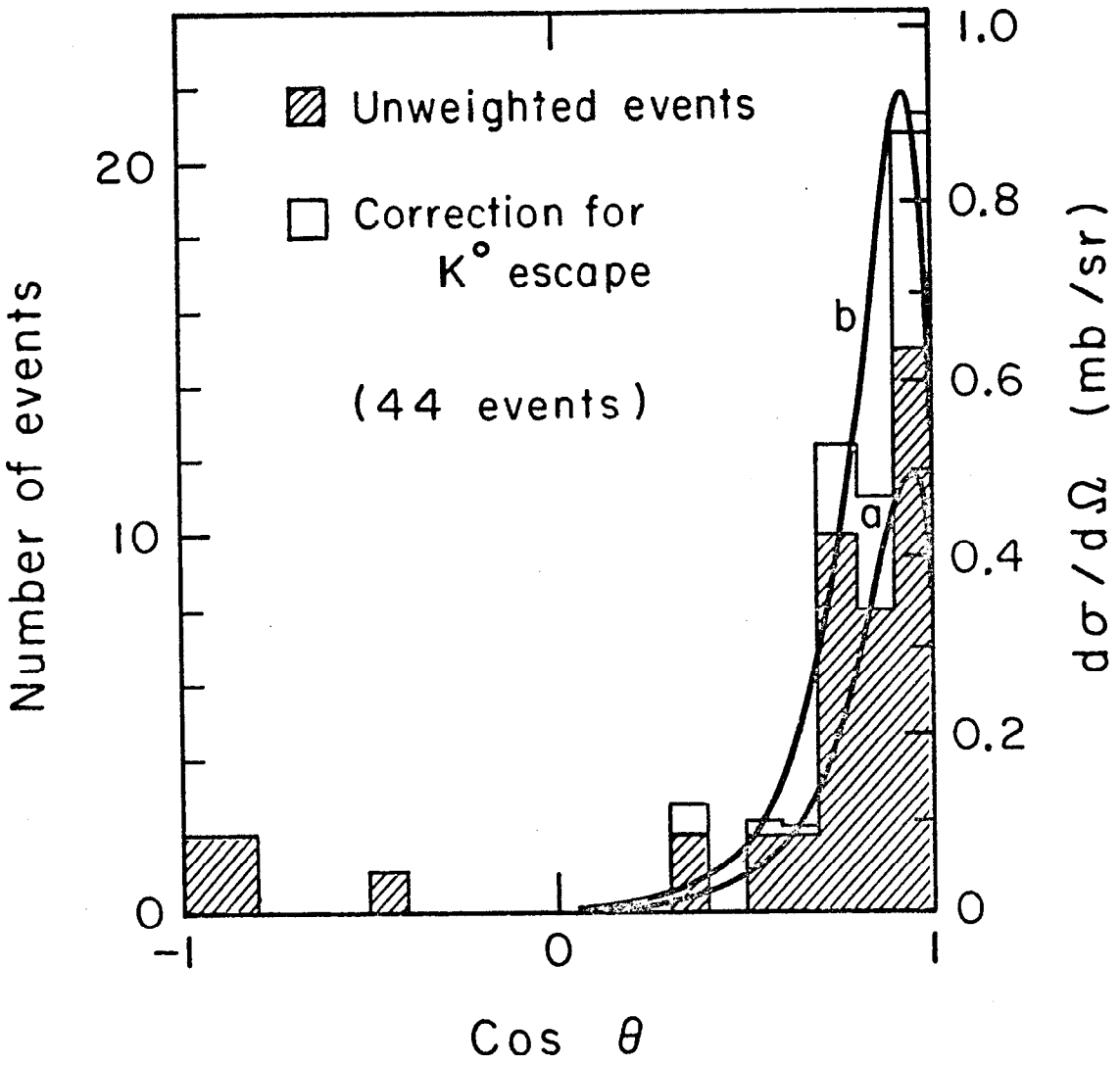

MUB-11563

Figure 5

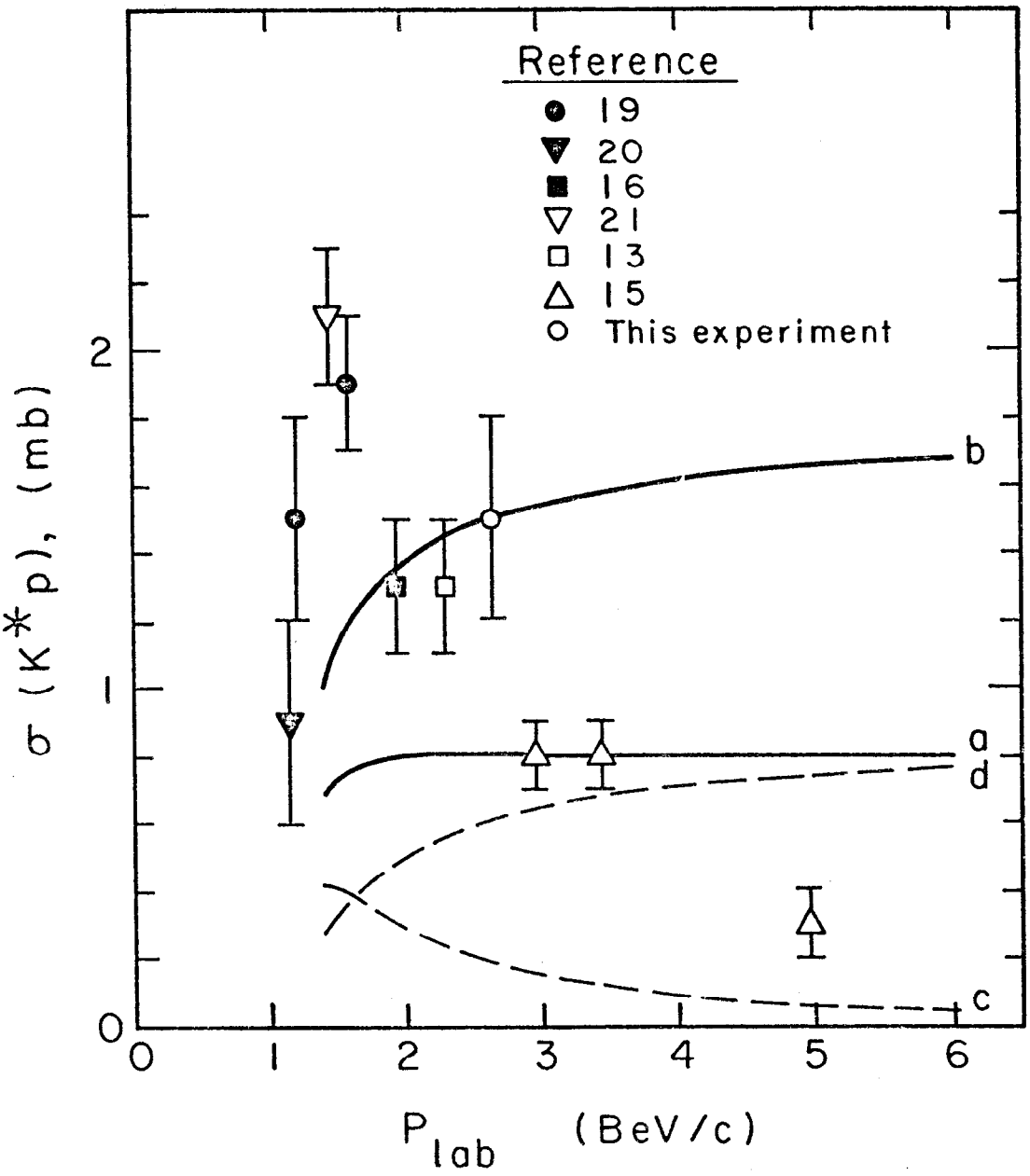

MUB-11564

Figure 6

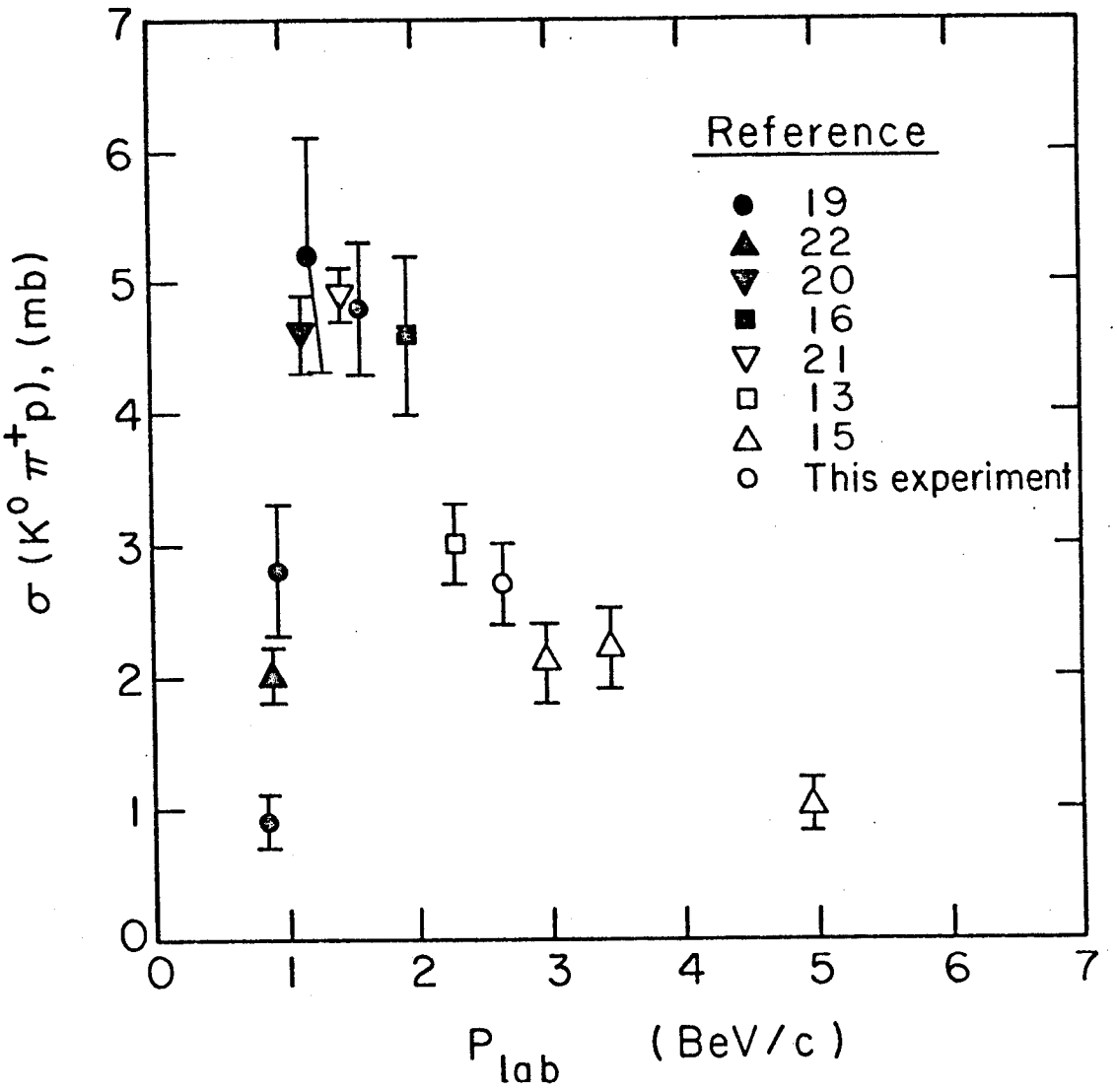

MUB-11565

Figure 7

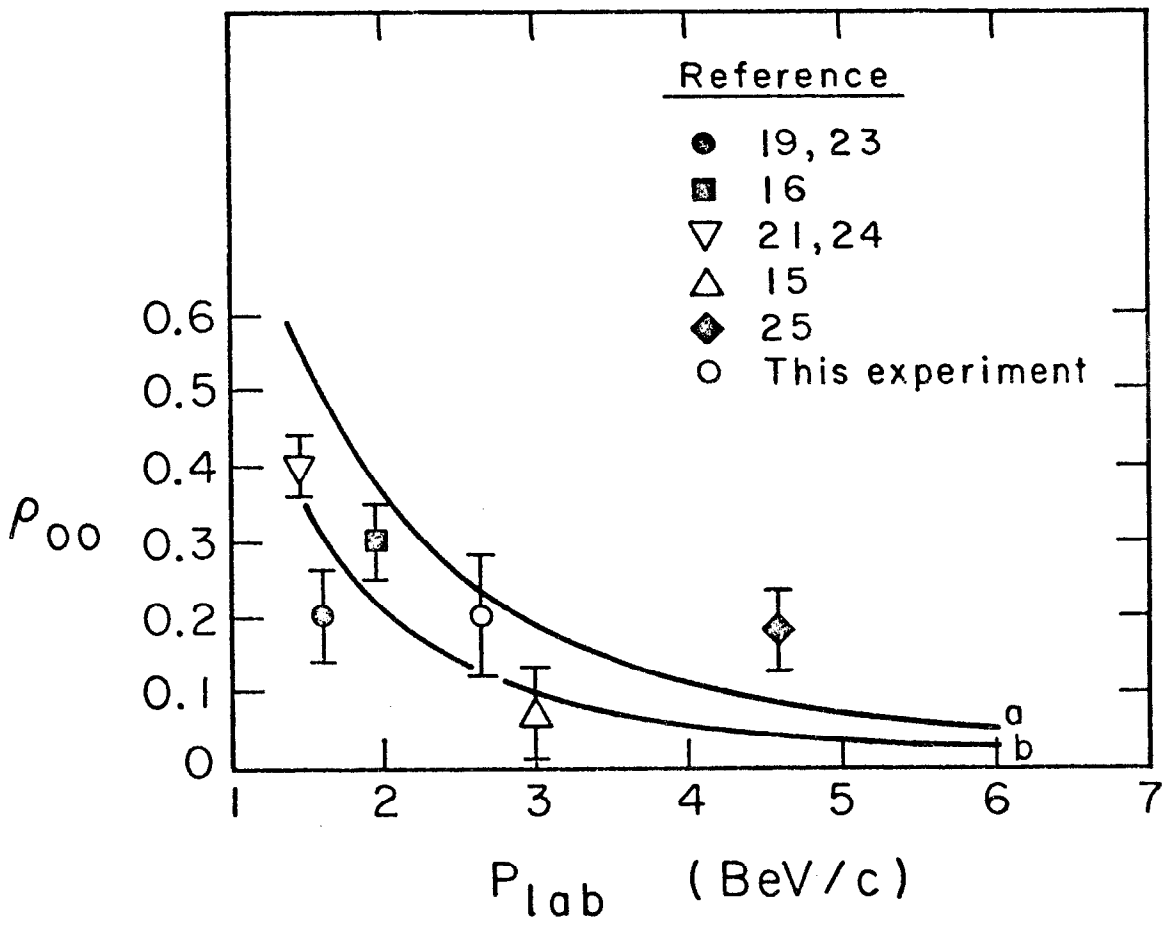

MUB 11566

Figure 8

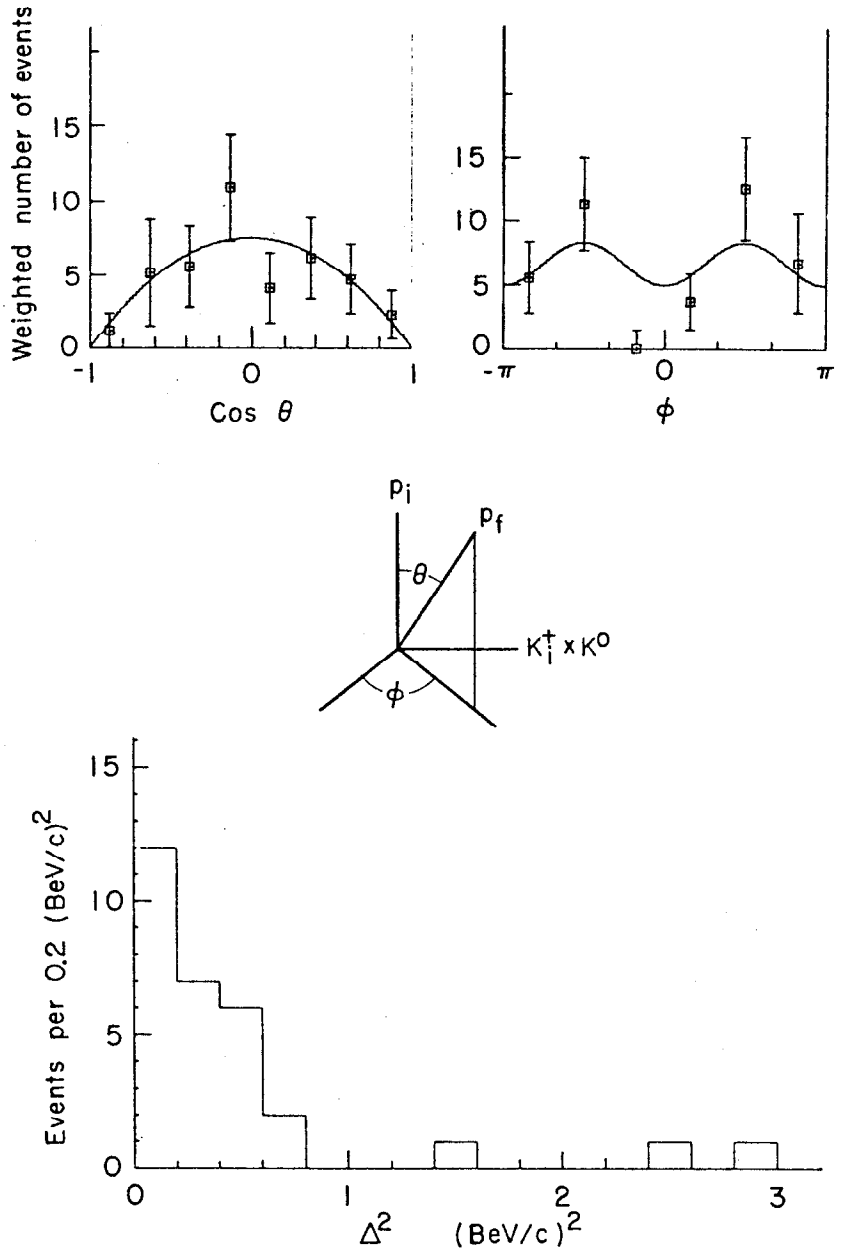
Weighted number of events
15
10
5
0
-1
0
1
Cos θ
15
10
5
0
-π
0
π
φ
p_i
p_f
θ
K_1^+ x K^0
φ
15
10
5
0
Events per 0.2 (BeV/c)^2
0
1
2
3
Δ^2 (BeV/c)^2
MUB-11404

Figure 9

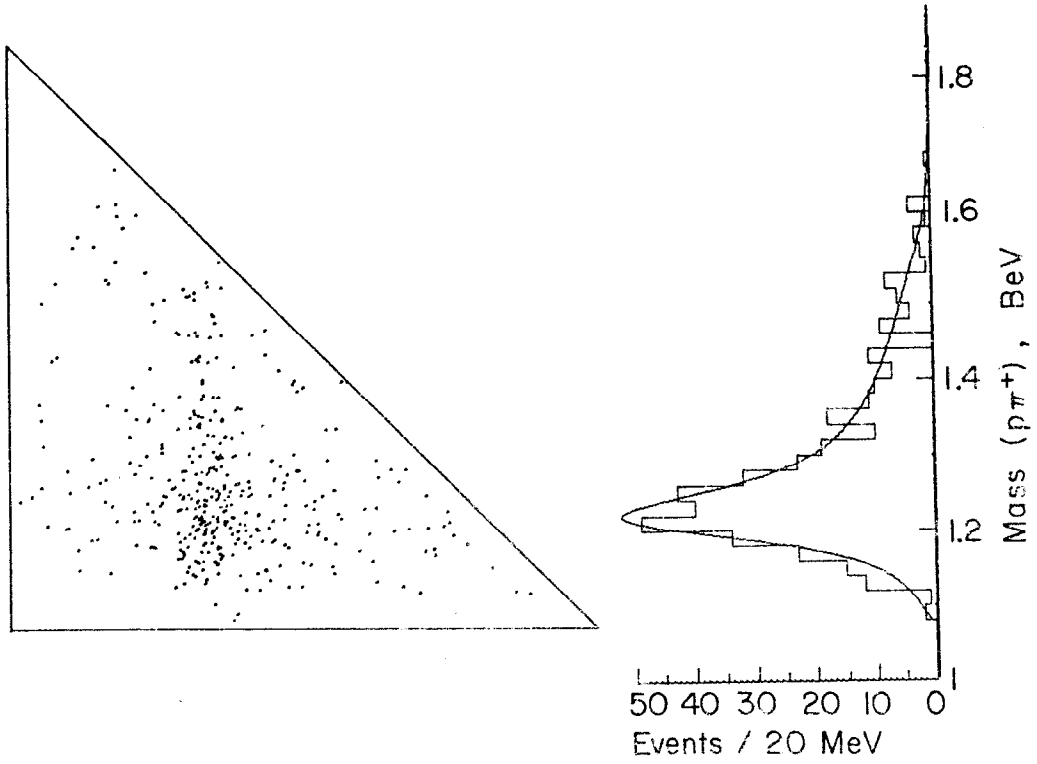

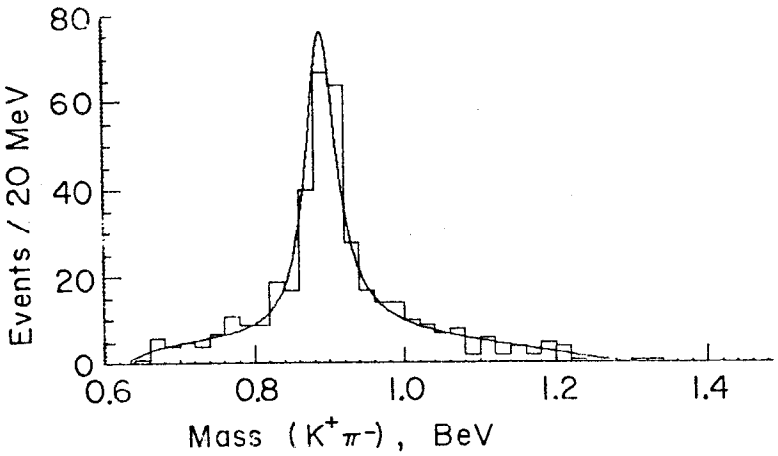

MUB-11444

Figure 10

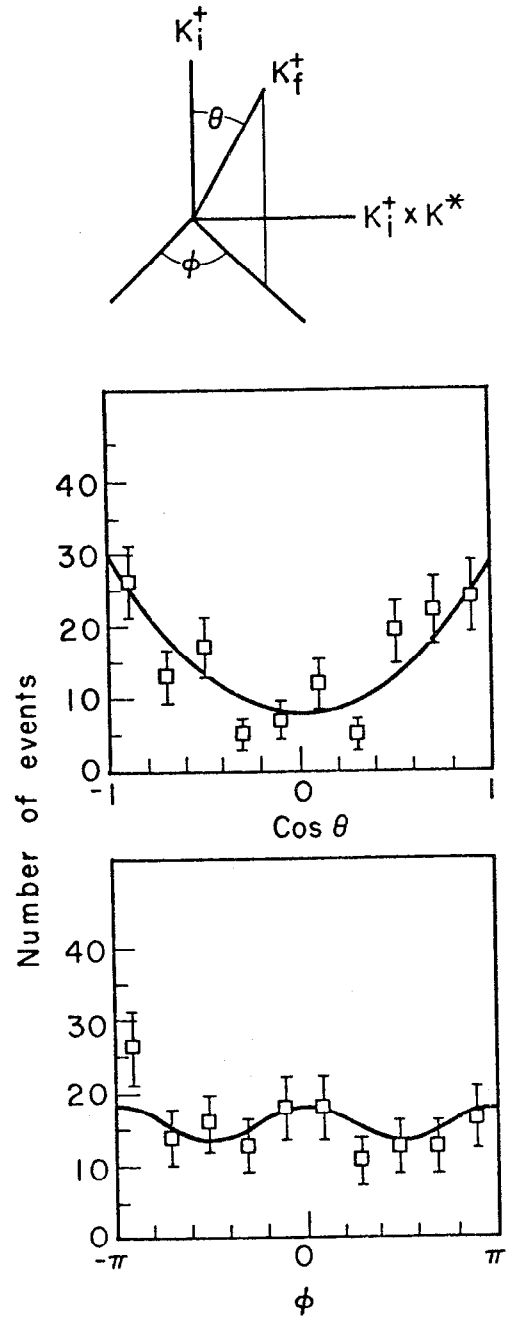

MUB-11442

Figure 11

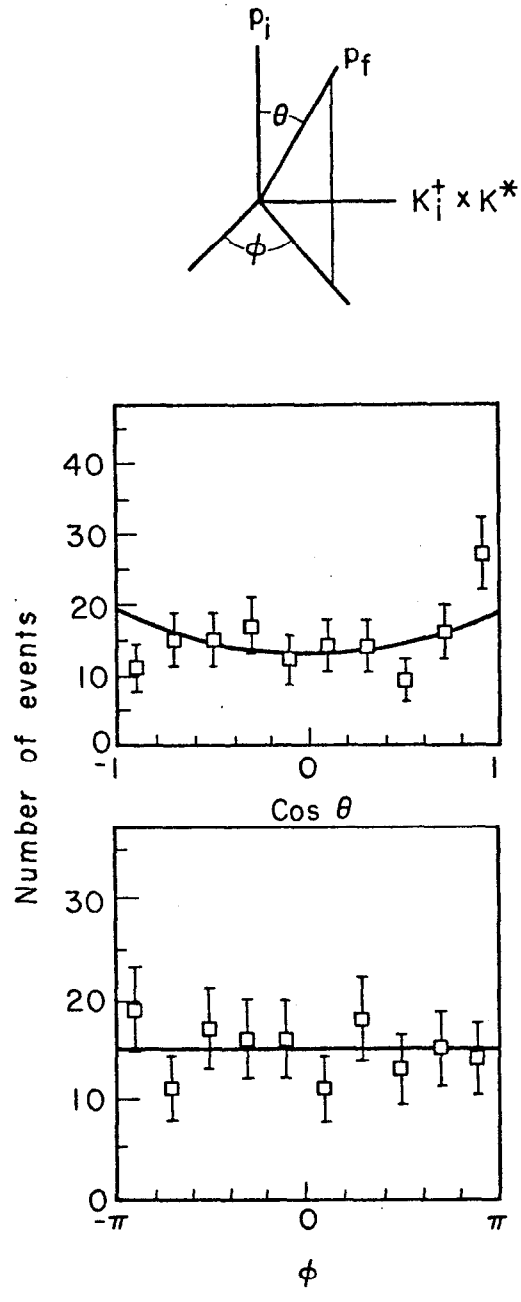
p_i
p_f
θ
$K_1^+ \times K^*$
ϕ
Number of events
40
30
20
10
0
-1
0
1
Cos θ
30
20
10
0
$-\pi$
0
π
ϕ
MUB-11441

Figure 12

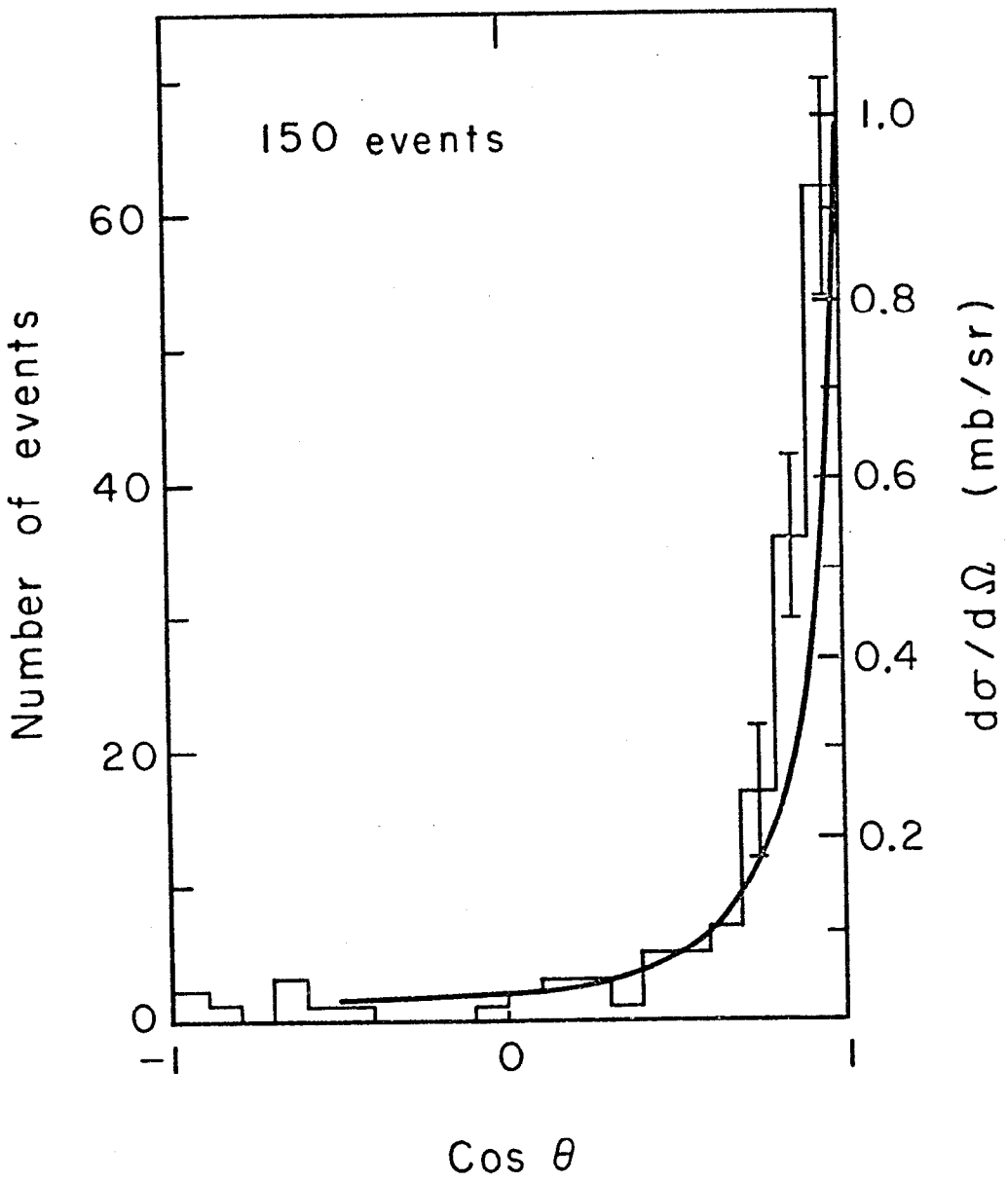

MUB 11567

Figure 13

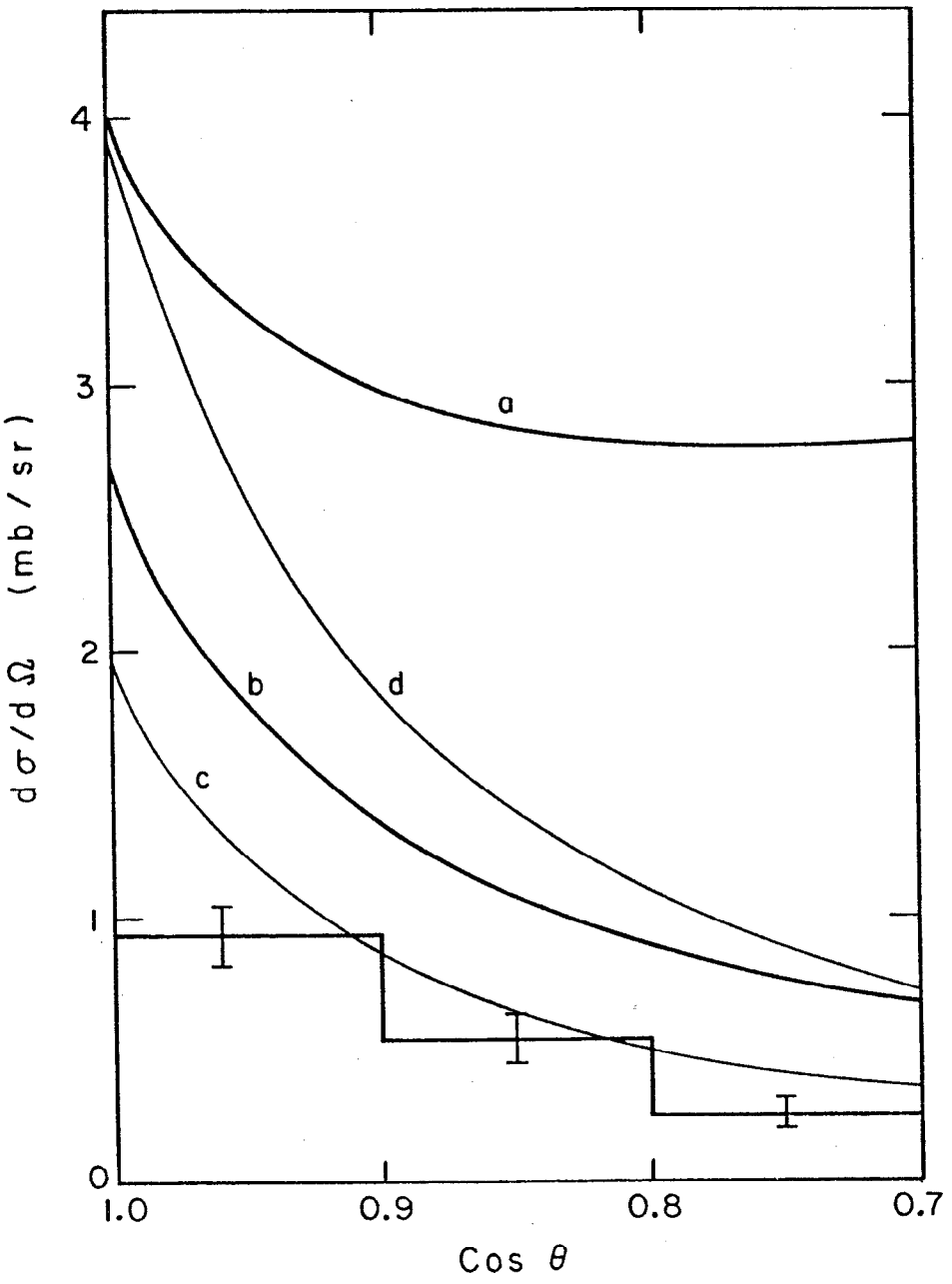

MUB-11569

Figure 14

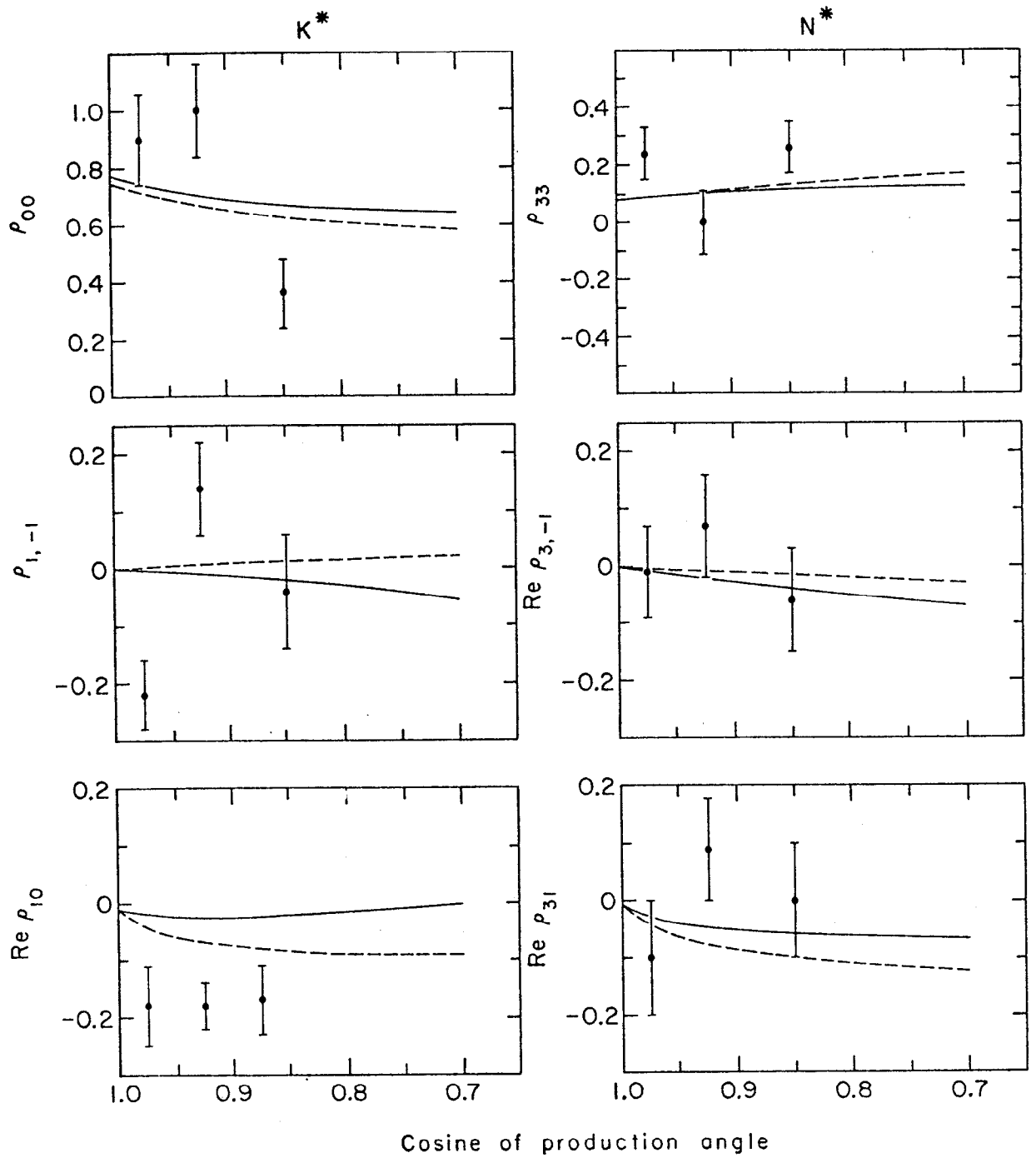
K*
N*
ρ_{00}
ρ_{33}
$\rho_{1,-1}$
Re $\rho_{3,-1}$
Re ρ_{10}
Re ρ_{31}
1.0
0.8
0.6
0.4
0.2
0
-0.2
-0.4
0.9
0.7
Cosine of production angle
MUB 11570

Figure 15

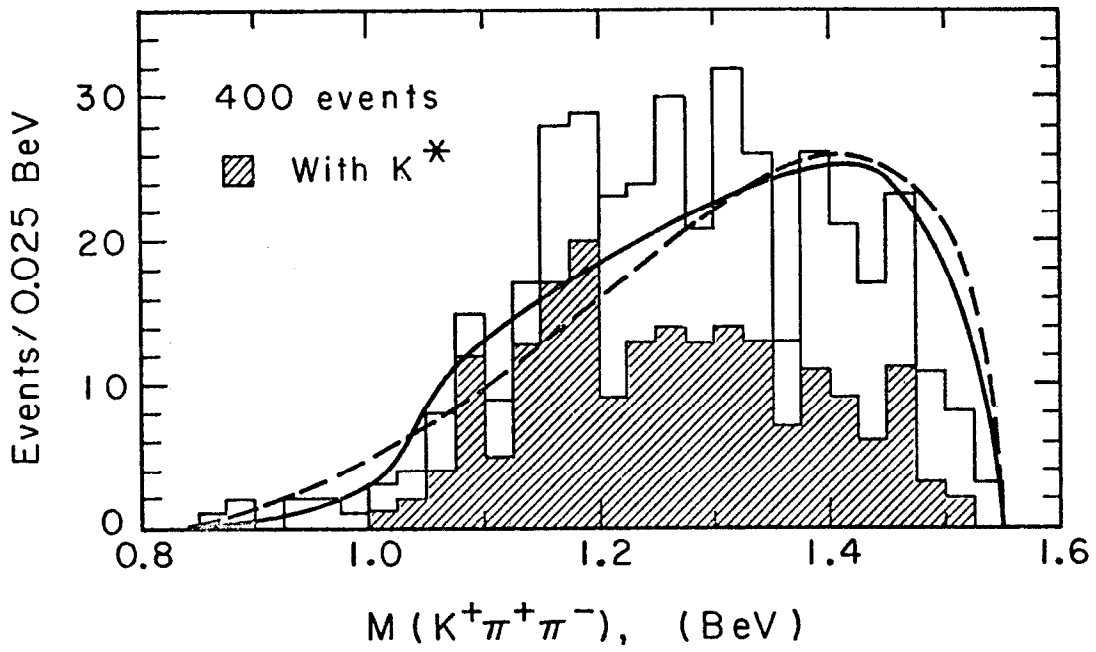

MUB 11568

Figure 16